2021

Characterizing the Geomagnetic Field at High Southern Latitudes: Evidence From the Antarctic Peninsula

Joseph Biasi
Dartmouth College, joseph.a.biasi@dartmouth.edu

Joseph Kirschvink
California Institute of Technology

Roger Fu
Harvard University

JGR Solid Earth

RESEARCH ARTICLE
10.1029/2021JB023273

Characterizing the Geomagnetic Field at High Southern Latitudes: Evidence From the Antarctic Peninsula

Joseph Biasi[1,2,3], **Joseph L. Kirschvink**[1,4], **and Roger R. Fu**[5]

[1]Division of Geological and Planetary Sciences, California Institute of Technology, Pasadena, CA, USA, [2]Department of Earth Sciences, Dartmouth College, Hanover, NH, USA, [3]Department of Earth Sciences, University of Oregon, Eugene, OR, USA, [4]Earth-Life Science Institute, Tokyo Institute of Technology, Tokyo, Japan, [5]Department of Earth and Planetary Sciences, Harvard University, Cambridge, MA, USA

Abstract Due to a dearth of data from high-latitude paleomagnetic sites, it is not currently clear if the geocentric axial dipole (GAD) hypothesis accurately describes the long-term behavior of the geomagnetic field at high latitudes. Here we present new paleomagnetic and paleointensity data from the James Ross Island (JRI) volcanic group, located on the Antarctic Peninsula. This data set addresses a notable lack of data from the 60°–70°S latitude bin and includes 251 samples from 31 sites, spanning 0.99–6.8 Ma in age. We also include positive fold, conglomerate, and baked contact tests. Paleointensity data from three methods (Thellier-Thellier, pseudo-Thellier, and Tsunakawa-Shaw) were collected from all sites. The Thellier-Thellier method had low yields and produced unreliable data, likely due to sample alteration during heating. Results from the Tsunakawa-Shaw and pseudo-Thellier methods were more consistent, and we found a bimodal distribution of paleointensity estimates. Most sites yielded either <15 μT or >40 μT, which together span a range of estimates from long-term geomagnetic field models, but do not favor any model in particular. Alternating-field demagnetization of these samples, when combined with preexisting data, yields a revised paleomagnetic pole of −87.5°, 025°, $\alpha 95 = 3.6°$ for the Antarctic Peninsula over the last ~5 Ma, which suggests that the current data set is sufficiently large to "average out" secular variation. Finally, the C2r/C2n transition was probably found at a site on JRI, and further geochronological and paleomagnetic study of these units could refine the age of this reversal.

Plain Language Summary In Antarctica, the history of Earth's magnetic field is not well understood, due to a lack of measurements. However, understanding the history of Earth's magnetic field is important, because it can help us understand the earth's core, which generates the magnetic field. Here we present new data from the James Ross Island (JRI) volcanic group, located on the northeastern tip of the Antarctic Peninsula. These data tell us how *strong* the earth's field was, and what *direction* it was pointing in the geologic past. We used 251 samples from 31 sites, spanning 0.99–6.8 million years ago in age. Only some of the samples were useful for determining how *strong* the field was. Most sites gave strengths of <15 microtesla (μT) or >40 μT. Earlier studies have tried to estimate how strong the field was at this location, and our results do not support or disprove any of the previous studies. Our data on the *direction* of the field suggests that the Antarctic Peninsula has not experienced large scale tectonic movement over the last five million years, and that our data set is large enough to capture a long-term average of the magnetic field direction in this area.

Key Points:

- New paleomagnetic and paleointensity data are presented from James Ross Island, Antarctica
- A new paleomagnetic pole for the Antarctic Peninsula is given for the last 5 Ma
- Paleointensity data from multiple methods show a bimodal distribution of results (<15 μT or >40 μT)

Supporting Information:

Supporting Information may be found in the online version of this article.

Correspondence to:

J. Biasi,
biasi@dartmouth.edu

Citation:

Biasi, J., Kirschvink, J. L., & Fu, R. R. (2021). Characterizing the geomagnetic field at high southern latitudes: Evidence from the Antarctic Peninsula. *Journal of Geophysical Research: Solid Earth*, *126*, e2021JB023273. https://doi.org/10.1029/2021JB023273

Received 18 SEP 2021
Accepted 11 DEC 2021

Author Contributions:

Conceptualization: Joseph Biasi, Joseph L. Kirschvink, Roger R. Fu
Data curation: Joseph Biasi
Formal analysis: Joseph Biasi
Funding acquisition: Joseph L. Kirschvink
Investigation: Joseph Biasi
Methodology: Joseph Biasi, Joseph L. Kirschvink
Project Administration: Joseph Biasi
Resources: Joseph L. Kirschvink
Supervision: Joseph Biasi
Validation: Joseph Biasi, Joseph L. Kirschvink, Roger R. Fu
Visualization: Joseph Biasi
Writing – original draft: Joseph Biasi
Writing – review & editing: Joseph Biasi, Joseph L. Kirschvink, Roger R. Fu

1. Introduction

1.1. The High-Latitude Geomagnetic Field

Although Earth's instantaneous magnetic field deviates from a geocentric axial dipole (GAD), the average geomagnetic field over $>10^5$ year timescales is thought to be well-approximated by the GAD model (Johnson & Constable, 1995; Johnson & McFadden, 2015; Merrill & McFadden, 2003). The idea of a GAD-like time-averaged magnetic field is supported by an abundance of directional and intensity data from mid- to low-latitudes sites (e.g., Cromwell et al., 2018; Evans, 2006; Johnson et al., 2008; Veikkolainen et al., 2014). However, data from high-latitude sites are far less abundant (Figure S1 in Supporting Information S1). Some studies suggest that magnetic field intensity near the poles is lower than expected from the GAD model during the last 5 My (Lawrence et al., 2009). Geomagnetic field models based in part on compilations of paleomagnetic data such as

Model G (McElhinny & McFadden, 1997) and TK03 (Tauxe & Kent, 2004) also include non-GAD geomagnetic field structure at these high latitudes. If these results are confirmed, the GAD hypothesis may not represent an accurate approximation of time-averaged magnetic field at high-latitude sites.

Accurately determining the long-term structure and behavior of the geomagnetic field is important for several reasons. The geomagnetic field itself is driven by convection in the Earth's core, so the structure of the field is informative of the structure and convection regime of the core (Glatzmaier & Roberts, 1995). For example, non-GAD components of the earth's geomagnetic field can be explained in part by the tangent cylinder (TC). This is a region of the outer core that is inferred to have a different convective regime than outside the TC. If current models of the TC are correct, high-latitude sites are expected to be most affected by variations within the TC—expressed as high- or low-flux regions at the earth's surface (e.g., Livermore et al., 2017). Furthermore, understanding the field at high latitudes can aid in interpretation of paleomagnetic data from high latitude sites. Paleogeographic reconstructions of Antarctica are uncertain (Milanese et al., 2019; Torsvik et al., 2007), but have significant climate implications. For example, Antarctica did not form large ice sheets until establishment of the Antarctic circumpolar current sometime in the Paleogene. However, the current formed after separation of Antarctica from South America, and the timing of this separation is uncertain (Hill et al., 2013; Scher et al., 2015).

Accumulating more high-latitude data is not an easy task. In the Arctic, most volcanism over the last 10 Ma has been due to seafloor spreading (Cottrell, 2015). This leaves Iceland and a few isolated islands as the only subaerial sites available for paleomagnetic study. In the Antarctic, volcanism is common in West Antarctica over the last 10 Ma (Smellie, 2021a). However, logistical challenges and ice cover has led to very few paleomagnetic studies (e.g., Lawrence et al., 2009; Oliva-Urcia et al., 2016). These problems are only compounded for older periods (>10 Ma), where the exposure of appropriately aged rocks is reduced, and the tectonic motion of Antarctica introduces additional uncertainties.

In typical paleomagnetic studies, the directional components of the ancient field vector (e.g., declination [D] and inclination [I]) can be extracted more easily than the paleointensity, due to the tendency of paleointensity samples to exhibit non-ideal thermal recording behavior and alteration during laboratory heating. Therefore, even fewer reliable measurements of high latitude paleointensities are available. The present-day geomagnetic field has a Virtual Axial Dipole Moment of ~80 ZAm^2, with expected surface intensities of ~30 μT at the equator and ~60 μT at the poles (Cromwell, Tauxe, & Halldórsson, 2015). Over the last 5 Ma, low- to mid-latitude sites give a variety of average intensities, but high-latitude sites show lower-than-expected intensities (Cromwell, Tauxe, & Halldórsson, 2015; Juarez et al., 1998; Lawrence et al., 2009; Tauxe et al., 2013). Some studies suggest that the long-term average GAD was roughly half the strength of the modern GAD, producing surface intensities of ~16 μT at the equator and ~32 μT at the poles (Juarez et al., 1998; Tauxe et al., 2013; Wang et al., 2015). However, very few high-latitude sites exist to validate these field models. At present, most of these studies have focused on Iceland (Arctic) or McMurdo Sound (Antarctic) (see Cromwell et al., 2018 for a compilation of relevant studies).

1.2. Previous Paleomagnetic Studies

One previous paleomagnetic study was done on the James Ross Island volcanic group (JRIVG) by Kristjánsson et al. (2005), focusing on use of paleomagnetic data for flow-correlation and volcanostratigraphy. They report alternating field (AF) demagnetization results from 15 sites (59 samples) with accompanying $^{40}Ar/^{39}Ar$ age data. For the JRIVG, they calculate a mean direction of $I = -76°$, $D = 352°$, and $\alpha_{95} = 7°$. Their flows range from 3.95–5.91 Ma in age.

Elsewhere on the Antarctic Peninsula (AP), a limited number of paleomagnetic studies have been done on units that are <10 Ma in age. In the South Shetland Islands, Scharnberger et al. (1982) report natural remanent magnetization (NRM) values from 2 sites, Blundell (1962) report AF demagnetization results from 5 sites, and Valencio and Fourcade (1969) report paleomagnetic results from 5 sites. More recently, Baraldo et al. (2003) report AF and thermal demagnetization results from 21 sites and Oliva-Urcia et al. (2016) report thermal demagnetization results from 20 sites on Deception Island spanning the last ~150 ka. Collectively, these results cover the last ~14 Ma, but are heavily biased toward data from Quaternary deposits on Deception Island. As a result, the average pole position from these data is offset from the geographic south pole (Oliva-Urcia et al., 2016), suggesting

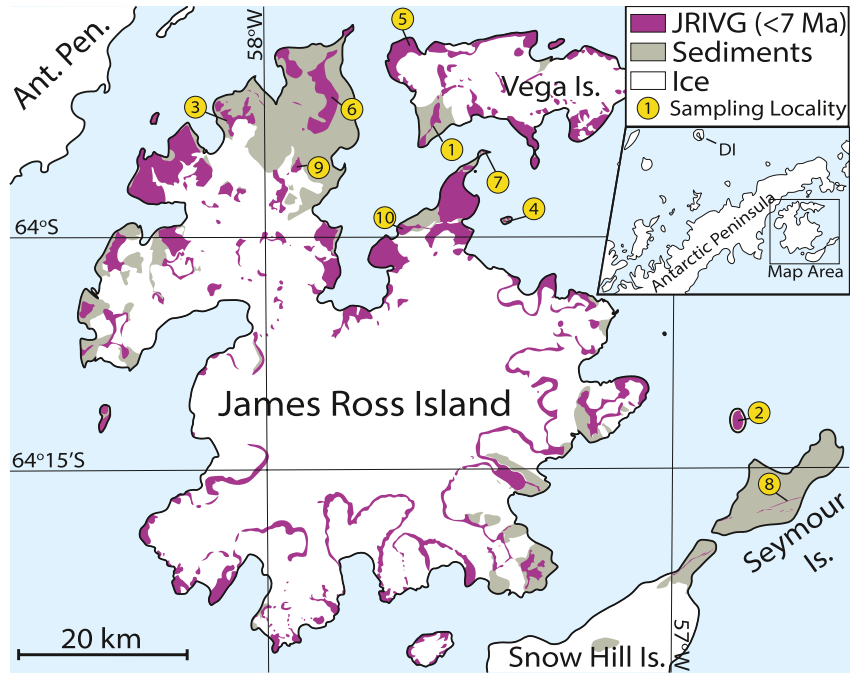

Figure 1. Simplified geologic map of James Ross Island and surrounding areas. Numbered sampling localities correlate with Table S1 Supporting Information S1. JRIVG = James Ross Island Volcanic Group. DI = Deception Island. Modified from Smellie et al. (2013).

that these data do not cover a long-enough time span to average-out paleosecular variation (Smellie, 2021b). In addition, no paleointensity data were gathered in these studies.

Comparatively, the volcanic deposits of McMurdo Sound are far better studied. The combined efforts of several studies (e.g., Lawrence et al., 2009; Mankinen & Cox, 1988; Tauxe et al., 2004; Turnbull, 1959) have provided directional and intensity data on >100 lava flows over the last 10 Ma. Of the studies listed above, a recent global compilation of high-quality paleomagnetic data has found that only some studies near McMurdo (Lawrence et al., 2009; Tauxe et al., 2004), and two studies at Deception Island (Baraldo et al., 2003; Oliva-Urcia et al., 2016) meet modern methodology and data quality standards (Cromwell et al., 2018). This leaves a dearth of reliable paleomagnetic data from the Antarctic, which are critical for construction of global geomagnetic field models in the recent and geologic past.

Here we report new inclination, declination, and absolute intensity measurements from the JRIVG on the northeastern tip of the AP (Figure 1). This data set provides directional and paleointensity constraints on the long-term behavior of the high-latitude geomagnetic field and is only the second data set of its kind (directions and intensity) in Antarctica after Lawrence et al. (2009). These data were derived from 28 igneous sites, and range in age from 0.99 to 6.8 Ma (Table S1 in Supporting Information S2). Finally, we use the paleomagnetic data collected in this study to refine the volcanostratigraphy of the JRIVG.

2. Geologic Background

2.1. Tectonic Setting

This study focuses on the JRIVG, located in the northeastern tip of the AP (Figure 1). This area is tectonically complex, with the timing of some events—such as the opening of the Drake Passage—remaining hotly debated (Eagles, 2004; Hill et al., 2013; Scher et al., 2015). The AP was originally part of Gondwana until ~125 Ma, when the Falkland plateau began separating from southern Africa (Jokat et al., 2003). The AP remained adjacent to the South American plate until the Eocene, when the continents separated, forming the Scotia plate, Drake Passage, and eventually the Antarctic circumpolar current (Dalziel et al., 2013). Subduction of (proto-) Pacific crust under the western side of the AP was ongoing from the Triassic to the Neogene, which was responsible for

voluminous arc magmatism on the peninsula (Doubleday et al., 1994; Pankhurst, 1982; Riley & Leat, 2021). Over the course of the Miocene, subduction ceased entirely along the AP (Livermore et al., 2020). Following cessation of subduction, small alkaline volcanoes appeared throughout the peninsula, including the JRIVG (Hole, 1988; Hole et al., 1991; Hole & Larter, 1993; Smellie, 1987; Smellie & Hole, 2021). Alkaline volcanoes on the west side of the AP appear to owe their origin to back-arc rifting and extension with some input from the subducting slab, though the origin of several volcanoes in this area is not well known (Haase & Beier, 2021; Smellie, 2021b). The JRIVG shows little slab input and is more similar to intraplate volcanism. Activity in this area is attributed to extension of thin continental lithosphere (Haase & Beier, 2021; Smellie, 2021b).

2.2. James Ross Island

James Ross Island (JRI) has been relatively well-studied compared to typical Antarctic localities due to the presence of nearby Argentinian, Czech, and Chilean bases, which facilitate frequent visits by scientists from these countries as well as American and British scientists. The geology of the area has been the subject of numerous studies, most of which focused on igneous petrology (e.g., Košler et al., 2009; Sykes, 1988), geochronology (compilation of ages in Smellie, 2021b), glaciology (Carrivick et al., 2012; Engel et al., 2012), sedimentology/stratigraphy (Milanese et al., 2020; Tobin et al., 2012, 2020), and paleontology (Olivero, 2012; Roberts et al., 2014). The area consists of a thick Cretaceous-Paleogene sedimentary basin, capped by a large basaltic polygenetic shield volcano along with several smaller outlying volcanoes (Figures 1 and 2a) (Smellie et al., 2013). These units are variably covered by ice caps and glaciers, which are rapidly retreating in most cases (Engel et al., 2012; Smellie et al., 2013). The nearest exposures of crystalline basement rocks are on the AP.

Volcanic rocks of the area comprise the JRIVG, and consist of hundreds of basalt flows, scoria cones, stocks, dikes, plugs, sills, and hyaloclastite foresets. Eruptive products were variably subaerial, subaqueous, and subglacially emplaced (Smellie, 2021b). Mt. Haddington, which makes up a large portion of JRI, is also the largest volcano in Antarctica both in terms of basal diameter (60–80 km) and total volume (4,500 km^3). For comparison, the more well-known Mt. Erebus volcano on Ross Island (near McMurdo station) is less than half the size, with a basal diameter of ∼40 km and total volume of 2,200 km^3 (Esser et al., 2004; Smellie, 2021b; Smellie & Martin, 2021). Volcanic activity began at >12 Ma, based on the oldest dated material from the JRIVG (a K-Ar age; Marenssi et al., 2010). The volcanostratigraphy and age-relations between the most easily accessible units have been well established over the course of several studies (e.g., Calabozo et al., 2015; Smellie et al., 2008), though several stratigraphic uncertainties are still present for more inaccessible units.

3. Methods

3.1. Fieldwork and Sample Collection

We sampled a wide variety of igneous products for this study and did not limit ourselves exclusively to basaltic lava flows. Most sites were accessed via helicopter (Figure 2c), which was essential to reach the tops of most volcanic mesas in the area. Coastal sites were typically accessed via small boats. Cores (2.54 cm diameter) were drilled using a Pomeroy gas-powered drill with water-cooling and were oriented using multiple methods. A Pomeroy orienting tool (Figure 2b) was used on all samples while sun compass measurements were taken whenever possible to calculate declination corrections. Sightings to distant features were taken when sun compass measurements were not available. Typical declination corrections were ∼11.3°. No block samples were collected for this study. Specimens were cut from each core, which were typically 3–6 cm in height.

In total, 251 paleomagnetic cores were collected from 31 sites that spanned 0.99–6.8 Ma in age. A "site" is defined as one cooling unit such as a lava flow, dike, or sill. Multiple sites in the same area are grouped into "locations," which are shown in Figure 1. These samples were collected over the course of the six-week field season in February/March 2016. In addition, >1,000 cores were taken from Cretaceous-Paleogene sediments in the JRI area in the same timeframe, which are the subject of other studies (Milanese et al., 2019, 2020; Tobin et al., 2020). Igneous samples were targets of opportunity, as the Cretaceous sediments were the main focus of the expedition. As a result, a wide variety of volcanic and intrusive products were sampled, which are discussed below. No fresh volcanic glass was found at our sampling localities, which will become more relevant when discussing paleointensity results (see Section 5.4). Five sites were excluded from paleomagnetic pole calculations because they are not in-place and have undergone an uncertain amount of rotation or tilting since acquiring their

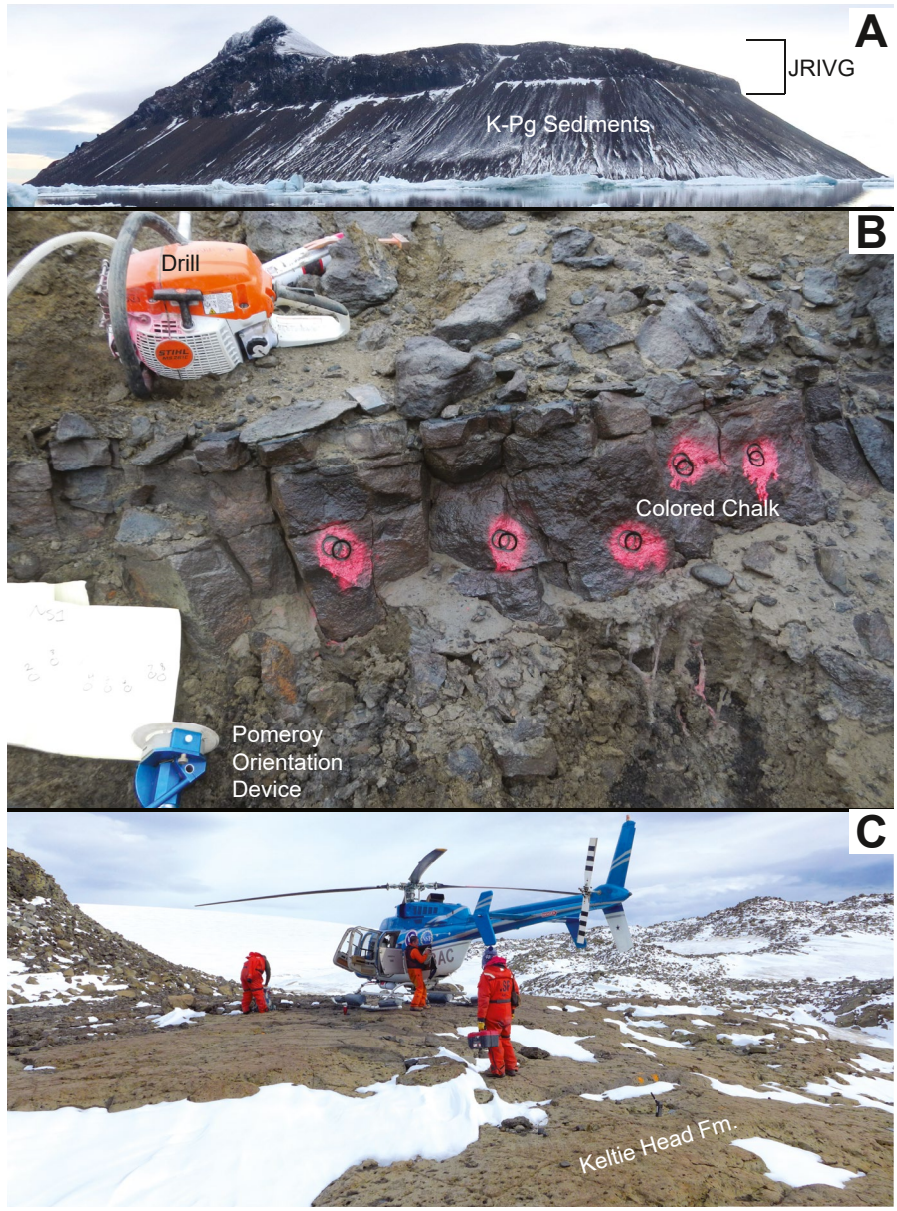

Figure 2. (a) Field photo of Cockburn Island (looking northeast), showing the typical relationship between the JRIVG and the underlying sedimentary rocks. (b) Field photo of a small sill at The Naze, showing typical drilling and orienting equipment. Note that the chalk is non-toxic and water soluble, and lasts at most one or two seasons. Photo credit: Sarah Slotznick. (c) Photo of a typical lava flow at Keltie Head. Most flows are >1 Ma in age and no longer have glassy or well-preserved flow tops. Helicopter support was essential to reach most sites in this study.

original magnetizations. This includes the Smellie Peak landslide block (used for a fold test), and the pillow and dike sites on Cape Lamb (see Section 4.3.2).

3.2. Rock Magnetic Characterization

Representative samples were subjected to a range of rock magnetic analyses, which are described in Kirschvink et al. (2008). These tests are done to better understand the magnetic mineralogy of the samples, which can aid in interpretation of their corresponding paleomagnetic and paleointensity data. This includes progressive AF demagnetization of the NRM up to 120 mT followed by progressive anhysteretic remanent magnetization (ARM) and isothermal remanent magnetization (IRM) acquisition experiments, modified Lowrie-Fuller tests (Johnson

et al., 1975; Lowrie & Fuller, 1971), and Fuller test of NRM (Fuller et al., 2002). All samples were analyzed using a 2G Enterprises vertical SQUID magnetometer and custom ARM/IRM/AF coil setup at the California Institute of Technology. The magnetometer is housed in a shielded room with a background field of ∼150 nT.

Measurements of thermal-susceptibility curves were performed with an AGICO Multi-Function Kappabridge instrument. The samples were heated from room temperature at a rate of 9°C/minute and an operating frequency of 976 Hz. Maximum temperatures reached were 700°C, and all experiments were run in an argon atmosphere to minimize oxidation effects. Background "noise" was removed via the subtraction of a blank sample (run under identical conditions) using AGICO's *Cureval* software. Hysteresis loops were measured at the Tokyo Institute of Technology on a Princeton Instruments MicroMag 3900 vibrating sample magnetometer at room temperature, in fields from −1 to 1 T.

3.3. Paleomagnetic Measurements

All samples were measured on a 2G Enterprises vertical SQUID magnetometer with RAPID automatic sample changer (Kirschvink et al., 2008). After initial NRM measurement, samples were subjected to two thermal cycling steps to 77 K in liquid-nitrogen baths in a magnetically shielded vessel (<10 nT in a mu-metal can) for ∼15 min to remove viscous components that are carried by multi-domain magnetite (Muxworthy & McClelland, 2000). Samples were then demagnetized using a 20-step alternating field demagnetization protocol (1.6–90 mT; see Section 4.3.1). Sample analysis and best-fit determinations were done using the DemagGUI program as part of the PmagPy software package (Tauxe et al., 2016). Maximum angle of deviation (MAD) is reported to assess goodness of fit (Kirschvink, 1980) (Table S3).

3.4. Paleointensity Experiments

3.4.1. Thellier-Thellier

In addition to AF demagnetization experiments, we also performed Thellier-Thellier (TT), Pseudo-Thellier (PTT), and Tsunakawa-Shaw (TS) paleointensity experiments on subsets of our samples. For our TT experiments (Thellier & Thellier, 1959), we used the same methods and selection criteria of Lawrence et al. (2009), in order to directly compare the two Antarctic datasets (Table S4 in Supporting Information S2). After measuring NRMs, and as noted above, each sample was subjected to two liquid nitrogen baths in an attempt to reduce the effects of multidomain grains on later paleointensity experiments. Each Thellier-Thellier experiment then consisted of 11 in-field/zero-field or zero-field/in-field steps (the IZZI protocol; Yu et al., 2004), at 0°–600°C. In addition, four pTRM and four pTRM-tail checks were also performed to identify alteration of the samples. All heating steps were done in a magnetically shielded oven within a nitrogen atmosphere to minimize oxidation of the samples. In-field steps were done within a 40 μT bias field along the axis of the cores. Overall, the Thellier-Thellier experiments yielded unreliable results, which is discussed in Section 4.4.1.

3.4.2. Pseudo-Thellier

Pseudo-Thellier experiments (Tauxe et al., 1995) were also performed. Unlike the TT technique, this technique involves no heating steps. Instead, the NRM is progressively AF demagnetized, followed by progressively imparting an ARM, and then AF demagnetizing the new ARM. Two new calibrations of the technique were used here, and we have delineated which samples pass the de Groot et al. (2013) and Paterson et al. (2016) selection criteria in Table S5 in Supporting Information S2. We used a 40 μT bias field when imparting ARMs. These samples were also subjected to two liquid nitrogen baths prior to AF demagnetization.

3.4.3. Tsunakawa-Shaw

TS experiments were performed using the methods and selection criteria of Yamamoto and Yamaoka (2018) (Table S6 in Supporting Information S2). This method is complex and involves AF-demagnetization and low-temperature demagnetization of NRM, two TRM-imparting heating steps, and six ARM-imparting steps. The technique is also known as *low-temperature demagnetization, double heating technique, Shaw* or LTD-DHT-Shaw. The AF demagnetization steps used here are the same as those used in the directional estimations. Laboratory TRMs were imparted by heating samples to 610°C for 10–20 min and cooling them in a uniform field of 30 μT. ARMs were imparted with a DC bias field of 50 μT in the same direction as the laboratory TRM. Low-temperature

demagnetization steps, which are performed before the first AF demagnetization and after imparting the second ARM, were conducted in a similar manner as previously described.

4. Results

4.1. Sampling Sites

Observations, photos, and descriptions of each of the field sites are available in the Supplementary Material. A baked contact test was performed on a dike in the Sandwich Bluff Formation (Figure S6 in Supporting Information S1), a conglomerate test was performed on brecciated pillow basalts in the Smellie Peak Fm. (Figure S3 in Supporting Information S1), and a fold test was performed on a landslide block near Smellie Peak (Figure 1(9)). See Section 4.3.2 for stability test results.

4.2. Rock Magnetism

Results from rock magnetic experiments are summarized in Figures S7–S12 in Supporting Information S1. IRM acquisition curves (Figure S7 in Supporting Information S1) show moderate-strongly interacting grains, which agrees with results from ARM acquisition curves (Figure S8 in Supporting Information S1). There appears to be no systematic variability in particle interaction based on lithology. Some IRM derivative curves (Figure S7 in Supporting Information S1) have a single peak, suggesting that CLC 4, CLD 6, NS1 6, TBA 25, and TBA 30 have a single magnetic phase. Two peaks are present in the HIA 22, KLH 14, and LCH 2 acquisition curves, suggesting that two phases or mineral size distributions may be present in these samples.

Lowrie-Fuller tests (Lowrie & Fuller, 1971) show a mixture of results (Figure S9 in Supporting Information S1), with some samples showing L-type behavior (ARM is more stable; Xu & Dunlop, 1995), some showing H-type behavior (IRM is more stable), and some showing mixed behavior with crossing ARM and IRM curves. L-type samples include CLC 4, CLD 6, and TBA 30. The only H-type sample is NS1 6, and mixed samples include HIA 22, KLH 14, LCH 2, TBA 25. The mixed samples in Figure S9 in Supporting Information S1 largely overlap with samples showing multiple phases in Figure S7 in Supporting Information S1. NRM is of greater or equal resistance to AF demagnetization as ARM and IRM, with the exception of HIA 22 which shows substantial NRM decay (Figure S9c in Supporting Information S1), likely due to alteration to maghemite or Fe-oxyhydroxides. L-type behavior can indicate either a small (single-domain) grain size or small dislocation density (Xu & Dunlop, 1995), while H-type behavior indicates the opposite. Once again there appears to be no systematic variation in Lowrie-Fuller results by rock type.

Fuller test results (Fuller et al., 1988) are shown in Figure S10 in Supporting Information S1. For thermal remanent magnetization, a ratio of NRM:IRM of 1:100 or greater is expected. In igneous rocks, ratios of 1:1,000 or less are indicative of sample alteration (Fuller et al., 2002). Five samples (KLH 14, LCH 2, NS1 6, TBA 25, and TBA 30) show evidence for little-moderate alteration in these plots. Three samples (CLC 4, CLD 6, and HIA 22) show evidence for more substantial alteration based on lower NRM:IRM ratios, which is in agreement with field observations of the sampling sites (e.g., hydration and devitrification of volcanic glass).

Hysteresis loops are shown in Figure S11 in Supporting Information S1. Three samples (CLC 4, SEA 3, and TBA 30) show evidence for a strong paramagnetic component (Tauxe et al., 1996). Sample CLC 4 is a palagonite breccia, which by its very nature is an altered material (Nayudu, 1964), so we attribute the paramagnetism in this sample to alteration of magnetite to lepidocrocite or similar hydrous iron-oxides (Guyodo et al., 2016). Sample SEA 3 also showed evidence for alteration in the field (see Section S1 in Supporting Information S1), so we again attribute this to alteration. Finally, sample TBA 30 is from a palagonite tuff cone on Taylor Bluff. This cone appears to have been near the surface since its eruption and may have erupted into thin ice or a similarly wet environment, so we again attribute this to alteration. The remaining samples show somewhat similar hysteresis loops that are consistent with a mixture of single domain, pseudo-single domain, and paramagnetic material (Tauxe et al., 1996).

Finally, thermal-susceptibility curves (Figure S12 in Supporting Information S1) show that several samples have Fe-oxyhydroxide components, as evidenced by dissimilar heating and cooling curves (Gehring & Hofmeister, 1994; Minyuk et al., 2011; Özdemir & Dunlop, 1996). Samples CLC 4, HIA 22, NS1 6, and TBA 30 show evidence for dehydration of Fe-oxyhydroxides (e.g., goethite) upon heating, which are irreversibly altered

to form (titano)magnetite that is stable upon cooling (Minyuk et al., 2011). It is important to note that all samples clearly retain a portion of their original magnetite, as evidenced by drops in susceptibility around 580°C. The remaining samples show fairly similar heating and cooling curves, though the absolute value of the susceptibility is typically higher after heating due to annealing of grains (Bowles et al., 2013).

Overall, the rock magnetic data presented here show notable differences between samples from lava flows and all other volcanic products. Lava flow samples are generally less susceptible to alteration and show less evidence for paramagnetic material. Based on results from the IRM acquisition and thermal-susceptibility experiments, the flows contain magnetite and a Ti-rich titanomagnetite phase (possibly ulvöspinel). Samples from other settings have undergone varying degrees of alteration.

4.3. Paleomagnetic Directions

4.3.1. Demagnetization Results

Results from AF demagnetization are summarized in Figures 3 and 4, Figure S13 in Supporting Information S1, and Tables 1 and S3. In most cases, the samples were flipped every four AF steps to allow for running samples overnight on the RAPID system. This occasionally creates a zig-zag pattern in the orthogonal projections that can create artificially high MAD (Figure S14 in Supporting Information S1); this is most likely due to a few percent spatial heterogeneity of the side-saddle Helmholtz coil response functions used in the 2G magnetometers. If we had flipped each sample during every step, the additional averaging would reduce this small zig-zag behavior, which is evident when looking at thermal demagnetization data (Figure S14 in Supporting Information S1). When using a collection of independently oriented cores, however, these small errors average out, as shown from the precision parameter (K) values of our virtual geomagnetic poles (VGPs, Table 1). For example, best-fit directions from Lachman Mesa flow 2 are very similar when using AF demagnetization or thermal demagnetization data from TT experiments techniques (Figure S14 in Supporting Information S1). In the majority of cases, thermal demagnetization data cannot be used due to alteration of the samples during TT experiments (see Section 4.4.1), so we only use AF demagnetization data in our analysis.

As a result, when determining VGP positions, we do not include any samples with MAD >15°. At the site level, every site has at least two samples, and generally show lower intra-site scatter, which is expected for uncontaminated signal from volcanic rocks. The median K is 170, and is >50 for 21/25 sites (Table 1). The median $\alpha 95$ value is 4.2°. The main sources of high $\alpha 95$ values in our data set are either too few samples (Naze dike), eruption during a clearly transitional period (Cockburn Is. Flow 1, Taylor Bluff columns), or hydrothermal alteration (Humps Island).

VGPs from 25 sites are shown in Figure 4a, with normal polarity poles inverted to the southern hemisphere. To determine which poles are transitional (and therefore excluded from further calculations), we used the iterative cutoff calculation of Vandamme (1994). We found the Vandamme cutoff angle to be 34.9° (Table S2 in Supporting Information S2)—Poles above 55.1 or −55.1° latitude are therefore assumed to be normal or reversed, respectively. These are then averaged ($I = -76.9$, $D = 002.8$, $\alpha 95 = 4.0$) to create a paleomagnetic pole at −87.7°, 272.6° ($\alpha 95 = 7.0°$), which overlaps with the modern geographic north pole. This suggests that no significant tectonic movement of the AP has occurred over the last ∼5 Ma, and that our data set is large enough to average out secular variation.

Overprints are uncommon in our data set, with only 37/245 samples (15%) showing an overprint direction (Table S3). There appears to be no systematic variation (or lack of variation) in the overprint directions, and therefore little information can be gleaned from such data. Overall, despite sampling a wide variety of volcanic units, most samples were good carriers of a stable remanent magnetization.

4.3.2. Stability Tests

The JRIVG is very young by geologic standards, and as a result has not been tectonically rotated or regionally tilted and has not experienced regional metamorphism or folding. Despite this, we conducted a baked contact test, fold test, and conglomerate test to check for secondary magnetizations.

Using a landslide block, a fold-test (Graham, 1949) was performed near Smellie Peak. The block is roughly 200 m in thickness and ∼1 km in length, and probably was dislodged during a Holocene glaciation (Smellie

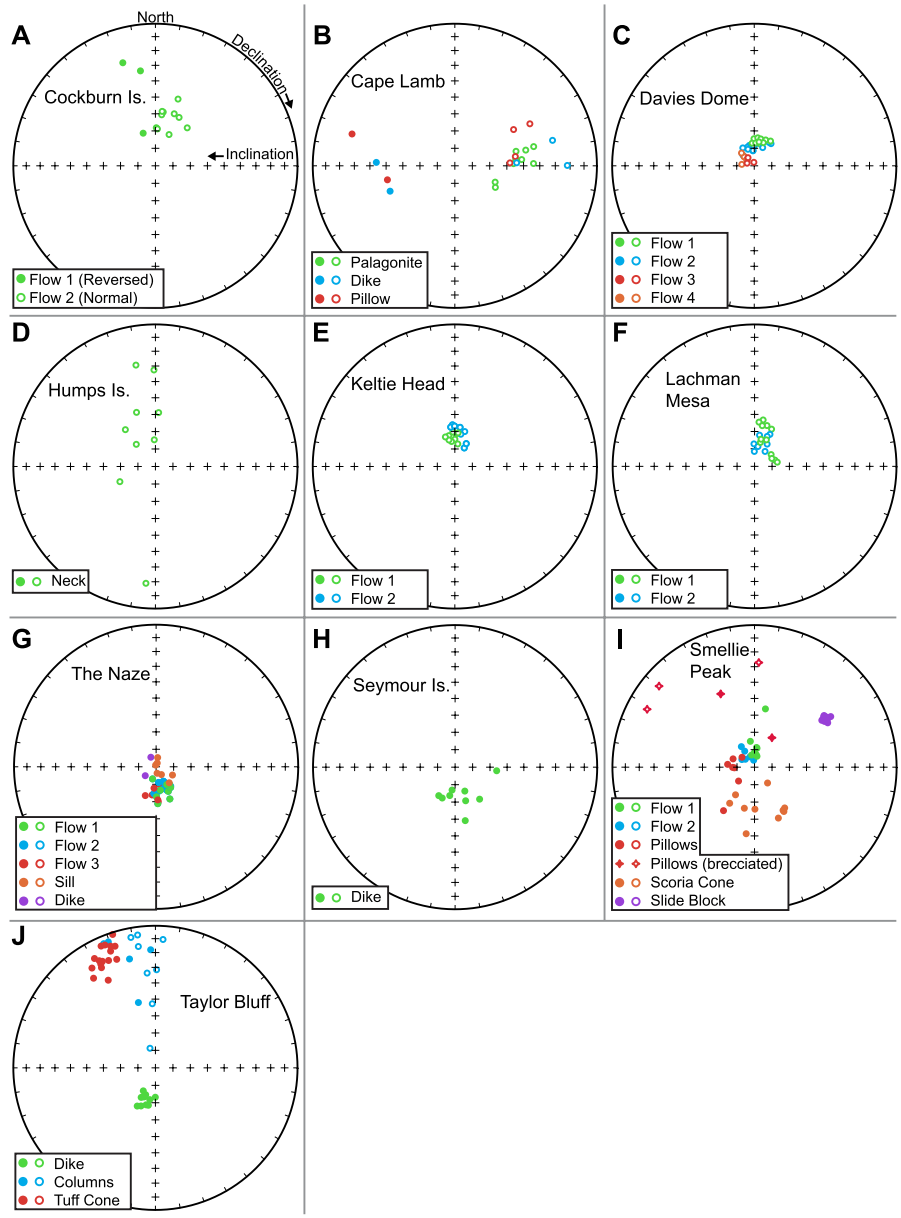

Figure 3. Equal area projections showing least-squares best fit directions from each site in this study. Negative inclination (normal polarity) samples are shown with hollow circles, positive inclination (reversed polarity) samples are shown with filled circles. The Cape Lamb pillow and dike, as well as the Smellie Peak slide block, are not in-place (Table 1). See Section 4.3.2 for discussion of these sites.

et al., 2008). The block is most likely from the Lookalike Peaks formation (Smellie et al., 2013), and yielded an average declination of 55.8° and inclination of 39.3° (without tilt-correction, Figure 3i), corresponding to a VGP of −6.4°, 352.5°. This direction differs significantly from any expected direction during a normal or reversed polarity period. Unfortunately, we were not able to sample an in-place section of the Lookalike peaks formation, so we cannot with 100% confidence state that the fold-test has been passed. However, it seems very unlikely that data of such consistency and quality ($k = 2{,}032$, $\alpha 95 = 0.9$) would be produced during a transitional period. The Lookalike Peaks formation erupted within the C3An (Gilbert) chron, and the determined age is not within error of a polarity transition (Ogg, 2020; Smellie et al., 2008). Furthermore, paleomagnetic data from the Lookalike Peaks Fm. was collected by Kristjánsson et al. (2005), who found typical reversed directions (Table S7 in Supporting Information S2). Similarly, data from the Smellie Peak area (another possible source of the block,

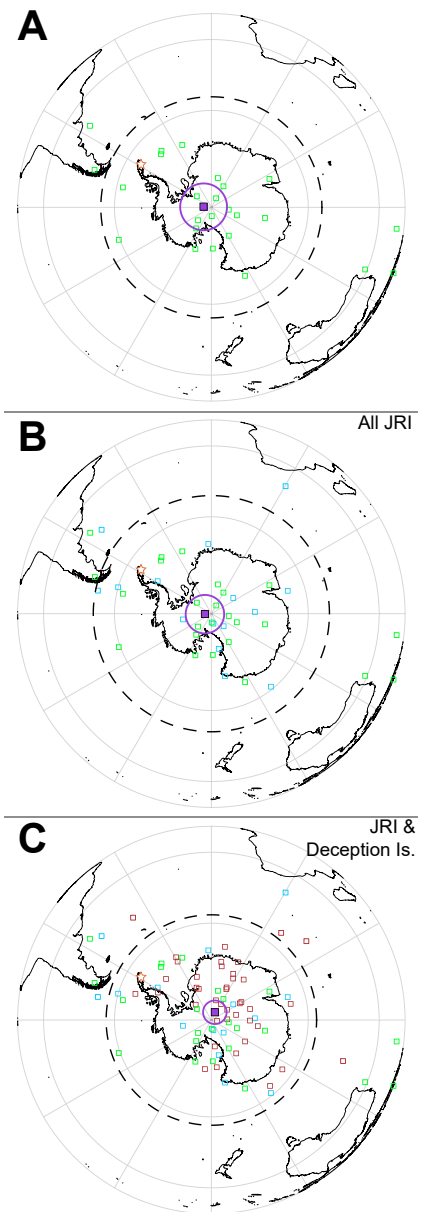

Figure 4. (a) Virtual Geomagnetic Poles (green) from this study. Dashed line is the iteratively calculated cutoff of Vandamme (1994). Purple square and circle are the average pole and α95 confidence interval, respectively. Orange star is the study site (James Ross Island). (b) Addition of VGPs from Kristjansson et al. (2005) (teal), with a recalculated cutoff angle and paleomagnetic pole. (c) Addition of young VGPs from Baraldo et al. (2003) and Oliva-Urcia et al. (2016) (red). Only sites that meet the PSV10 selection criteria of Cromwell et al. (2018) are included in the average pole (purple), but all sites are shown here. See Sections 5.1 and 5.2 for discussion.

Figure 3i) does not match the slide block's directions either. Therefore, we argue that the fold-test was successfully passed.

Using brecciated pillow basalts, a conglomerate test (Graham, 1949) was also performed at Smellie Peak. Samples SML 16, 17, 18, 19, and 27 were taken from brecciated pillows, while samples SML 20–26 were taken from in-place pillows in the same unit. The brecciated pillows show clearly distinct directions from the in-place pillows (Figure 3i, Table 1). Using the Watson (1956) test for randomness, we find a 95% likelihood that the directions from the brecciated pillows are random ($R = 3.45$, $R_0 = 3.50$, $P\text{-}value = 0.95$), indicating that the conglomerate test has passed.

Finally, we attempted a baked contact test (Graham, 1949) on a unique exposure of palagonite breccias, a dike, and a pillow basalt on Cape Lamb (Figure S6 in Supporting Information S1). The palagonite was a hyaloclastite breccia prior to low-temperature alteration (Drief & Schiffman, 2004). A dike can be seen directly feeding a pillow basalt at this exposure, but the dike is not very large, and we could not follow it beyond a few meters. Paleomagnetic data from all three units (Figure 3b) are rather unusual. The majority of the data show normal or transitional directions, while four samples from the dike and pillow show reversed or transitional directions. Most likely thermal overprinting of the dike and pillow by the hyaloclastite is responsible, as field photos indicate that all cores were marked correctly so the anomalous directions are unlikely to be a result of orientation errors. These hyaloclastite breccias can be emplaced at high temperature (Porreca et al., 2014; Yamagishi & Dimroth, 1985), and our consistent directions from the contact zone suggest that this is the case. The observed resetting would imply that the dike did not intrude the palagonite, and instead the palagonite incorporated the dike and pillow as a large clast during formation of the palagonite breccias. This is entirely possible from a volcanological perspective (Nayudu, 1964; Yamagishi & Dimroth, 1985), and the dike and pillow could have been produced in the same eruptive event as the hyaloclastite. Overall, we conclude that these results indicate a passing baked contact test, although not in the manner we originally anticipated.

4.4. Paleointensity

Paleointensity results are summarized in Figures S15–S17 in Supporting Information S1 and Table 2, Tables S8–S10 in Supporting Information S2. It is important to note that, due to access limitations, most (if not all) of our samples are not ideal paleointensity recorders. For example, no volcanic glass (the ideal paleointensity carrier in this case; Cromwell, Tauxe, Staudigel, & Ron, 2015) was collected, for the simple reason that we did not find any. Despite the non-ideal nature of our sample set, we deemed it worthwhile to conduct paleointensity experiments because of the near absence of such data from this latitude. Furthermore, we plan to use these data to guide paleointensity sampling during a future expedition to the JRIVG.

4.4.1. Thellier-Thellier

Success rates from Thellier-Thellier experiments were low (Table S8 in Supporting Information S2) with only 9/102 samples meeting the selection criteria of Lawrence et al. (2009) (Table S4 in Supporting Information S2), which are already lower than modern selection criteria standards (Cromwell, Tauxe, Staudigel, & Ron, 2015). Our low success rates are likely due to the presence of multidomain grains (indicated by two-component Arai plots) and Fe-oxyhydroxides. These minerals consistently de-watered during early stages of the experiments, which altered the "pTRM gained" significantly

Table 1
Site-Mean Virtual Geomagnetic Poles (VGPs)

#	Location	Site	Age[a]	*n*/*N*	*D*	*I*	a95	*K*	*R*	VGP Lat	VGP Lon	VGP dm	VGP dp	Polarity[b]
1	Cape Lamb	Palagonite	5.42 ± 0.08	9/9	87.3	-53.8	7.3	51	8.8	-31.6	226.9	10.2	7.1	Trans.
2	Cockburn Island	Flow 1	2.9 ± 0.4	3/3	345.4	42.5	38.8	11	2.8	-0.5	109.9	47.8	29.5	Trans.
2	Cockburn Island	Flow 2	2.9 ± 0.4	10/11	15.9	-61.7	5.1	89	9.9	-66.8	153.8	7.9	6.1	Normal
3	Davies Dome	Flow 1	5.36 ± 0.05	11/11	12.6	-76.7	2.1	473	11.0	-84.5	225.9	3.9	3.6	Normal
3	Davies Dome	Flow 2	5.36 ± 0.05	13/13	358.6	-79.3	2.8	227	13.0	-84.6	307.2	5.3	5.1	Normal
3	Davies Dome	Flow 3	5.36 ± 0.05	3/3	316	-86.2	4.1	903	3.0	-68.7	316.5	8.1	8.1	Normal
3	Davies Dome	Flow 4	5.36 ± 0.05	6/6	306.6	-82.9	2.1	973	6.0	-69.2	335.0	4.1	4.0	Normal
4	Humps Island	Plug	--	9/9	333.4	-67.6	26.5	5	7.3	-70.5	63.9	44.2	36.9	Normal
5	Keltie Head	Flow 1	0.99 ± 0.05	9/9	355.8	-73.3	2.2	562	9.0	-84.8	97.7	3.9	3.5	Normal
5	Keltie Head	Flow 2	0.99 ± 0.05	8/8	7.5	-70.5	4.1	184	8.0	-80.1	148.5	7.1	6.1	Normal
6	Lachman Mesa	Flow 1	5.04 ± 0.04	12/12	25.7	-73.1	5.2	71	11.9	-76.7	201.0	9.3	8.3	Normal
6	Lachman Mesa	Flow 2	5.04 ± 0.04	8/8	19.8	-76.0	3.6	244	8.0	-81.3	218.4	6.1	6.6	Normal
7	The Naze	Flow 1	–	9/9	163.8	75.9	3.8	184	9.0	-82.8	29.8	6.5	7.0	Reversed
7	The Naze	Flow 2	–	9/9	154.9	77.0	2.1	600	9.0	-79.2	14.3	3.6	3.9	Reversed
7	The Naze	Flow 3	–	7/8	184.6	75.3	4.2	203	7.0	-87.4	177.3	7.0	7.7	Reversed
7	The Naze	Sill	–	7/8	123.1	86.3	4.6	170	7.0	-67.1	318.6	9.1	9.1	Reversed
7	The Naze	Dike	–	2/2	272.4	85.4	24.2	109	2.0	-62.1	282.7	47.9	47.5	Reversed
8	Seymour Island	Dike	6.8 ± 0.5	8/9	176.2	71.7	6.6	72	7.9	-82.0	108.0	10.2	11.6	Reversed
9	Smellie Peak	Flow 1[c]	5.14 ± 0.38	9/9	3.3	78.1	5.7	83	8.9	-41.1	303.8	10.1	10.7	Trans.
9	Smellie Peak	Flow 2[c]	5.14 ± 0.38	6/6	322.8	82.3	3.4	382	6.0	-50.8	287.6	6.5	6.6	Trans.
9	Smellie Peak	Pillows	5.14 ± 0.38	7/7	256.4	77.3	8.4	53	6.9	-59.5	250.3	14.7	15.7	Reversed
9	Smellie Peak	Scoria Cone	5.91 ± 0.08	10/10	171.3	65.9	8.6	33	9.7	-73.6	101.2	14.0	11.5	Reversed
10	Taylor Bluff	Dike	1.94 ± 0.47	12/12	198.2	71.1	2.1	422	12.0	-77.7	178.0	3.7	3.2	Reversed
10	Taylor Bluff	Columns	2.03 ± 0.13	13/13	351.1	-10.8	18.4	6	11.0	-31.1	112.0	18.6	9.4	Trans.
10	Taylor Bluff	Tuff Cone	2.03 ± 0.13	16/17	335	15.5	4	87	15.8	-15.7	96.6	4.1	2.1	Trans.
Not in-place														
1	Cape Lamb	Dike (R)	5.42 ± 0.08	3/3	83.9	-35.4	28	20	2.9	-20.2	215.9	32.4	18.7	–
1	Cape Lamb	Dike (N)	5.42 ± 0.08	2/2	261.2	47.3	38.4	44	2.0	-29.1	218.2	49.8	32.3	–
1	Cape Lamb	Pillow (N)	5.42 ± 0.08	2/2	275.2	38.5	80.3	12	1.9	-17.1	226.8	95.3	56.6	–
1	Cape Lamb	Pillow (R)	5.42 ± 0.08	4/4	70.3	-51.1	13.8	45	3.9	-36.8	210.6	18.7	12.6	–
9	Smellie Peak	Pillow Breccia	5.14 ± 0.38	4/4	319.8	22.9	69.1	3	2.9	8.2	262.4	39.0	73.4	–
9	Smellie Peak	Slide Block	5.89 ± 0.09	14/15	55.8	39.3	0.9	2032	14.0	-6.4	352.5	1.1	0.6	–

Note. # = location on Figure 1; *n* = samples used; *N* = samples measured; *D* = declination; *I* = inclination; a95 = 95% confidence interval; *K* = precision parameter; *R* = vector sum; dm/dp = 95% confidence interval (elliptical); Trans. = transitional.

[a]See Table S1 in Supporting Information S1 for additional age information, see Smellie (2021b) for a compilation of ages from the JRIVG and associated references. [b]Transitional poles determined by Vandamme (1994) cutoff angle. [c]Tilt-corrected (160/18).

and caused the pTRM checks to fail in many samples. The TT results are reported in Table S8 in Supporting Information S2 and Figure S15 in Supporting Information S1 and show inconsistent results even within individual sites. Therefore, the results from this technique are not reliable and should not be incorporated into any regional or global data compilations. Recently, a statistical method has been developed to correct for multidomain behavior in Thellier-Thellier experiments (Cych et al., 2021). However, given the alteration that we observe in our samples during the experiments, such a method is not appropriate to apply to this data set.

4.4.2. Pseudo-Thellier

Pseudo-Thellier experiments had the highest success rates (Figure S16 in Supporting Information S1, Table S9 in Supporting Information S2) due to the lack of heating steps. Two sets of selection criteria were implemented here (Table S5 in Supporting Information S2). Of the two-hundred samples that were measured, 60 passed the selection criteria of de Groot et al. (2013) and 17 passed the more stringent selection criteria of Paterson et al. (2016). Only five samples passed both sets of selection criteria. In this case, we attribute most of our failed samples to multidomain and pseudo-single domain grain size, as dehydration of hydrous iron-oxides is not a factor in this technique.

Some sites show good internal consistency (Taylor Bluff tuff cone, Smellie Peak pillows) while other sites vary in their intensity estimations (Lachman Mesa flows). The relative intensities between sites with internally consistent results can be inferred from the PTT data. For example, the Taylor Bluff columns show consistently low intensity values (~5.5 μT) while Flow 1 at Keltie Head was probably erupted during a higher-intensity period (~66 μT). Several samples were successfully duplicated, meaning that multiple specimens from the same core passed the selection criteria. These duplications are all in agreement with each other (0.1%–4.8% differences in determined intensity), suggesting that errors associated with this technique are systematic, and do not significantly vary from analysis to analysis.

4.4.3. Tsunakawa-Shaw

Success rates from the TS method were between the TT and PTT success rates (Table S10 in Supporting Information S2), likely because the samples are only heated twice during this process. Of the 191 samples analyzed, 38 passed the selection criteria of Yamamoto and Yamaoka (2018) (Figure S17 in Supporting Information S1, Table S6 in Supporting Information S2). Within-site consistency is better than the TT results, but worse than the PTT results. Similar to the TT technique, we attribute failed samples to large grain size and alteration during heating. The TS intensities are generally higher than the TT intensities but are in very close agreement with the PTT intensities. More detailed discussion of these results is in Section 5.4.

5. Discussion

5.1. Combining JRI Data Sets

Paleomagnetic results from this study can be combined with the 15 sites from Kristjánsson et al. (2005) (Table S7 in Supporting Information S2) to create a combined paleomagnetic pole for the JRIVG. VGPs from both studies are shown in Figure 4b. The resultant paleomagnetic pole (−88.1°, 269.5°, $\alpha 95 = 5.8°$) appears to average-out secular variation and includes the geographic south pole in its envelope of uncertainty. Furthermore, several locations were sampled by both studies, and show good agreement (within error) in measured paleomagnetic directions (Table 1 and Table S7 in Supporting Information S2). Some minor variations between the two studies are likely due to sampling of different units at the same location, which will differ slightly in age. This pole also makes use of the Vandamme (1994) iterative cutoff technique to determine which VGPs are transitional (Table S2 in Supporting Information S2).

5.2. Incorporation Into the PSV10 Field Model

Given the young age of the JRIVG, paleomagnetic data from these units is most useful for incorporation into long-term models of the geomagnetic field, as there is little use of these data for tectonic reconstructions. As discussed previously, multiple paleomagnetic studies have been done on the AP, spanning the last ~14 Ma. However, a recent review of global paleomagnetic data by Cromwell et al. (2018) found that only two studies from Deception Island (Baraldo et al., 2003; Oliva-Urcia et al., 2016) met modern standards of data quality. An additional study by Kristjánsson et al. (2005) was not included in the above compilation. It also meets all of their criteria, but has not been uploaded into the MagIC database yet (https://www2.earthref.org/MagIC).

After combining site-level data from all four studies, the resultant paleomagnetic pole (−87.5°, 024.9°, $\alpha 95 = 3.6°$) is shown in Figure 4c. Again, the iterative cutoff of Vandamme (1994) was used here. Though the pole has a lower $\alpha 95$ uncertainty, it is also slightly farther from the geographic South Pole (compared to Figure 3b). This is caused by the Deception Island studies, which likely did not average-out secular variation. All of their sites are ~150 ka

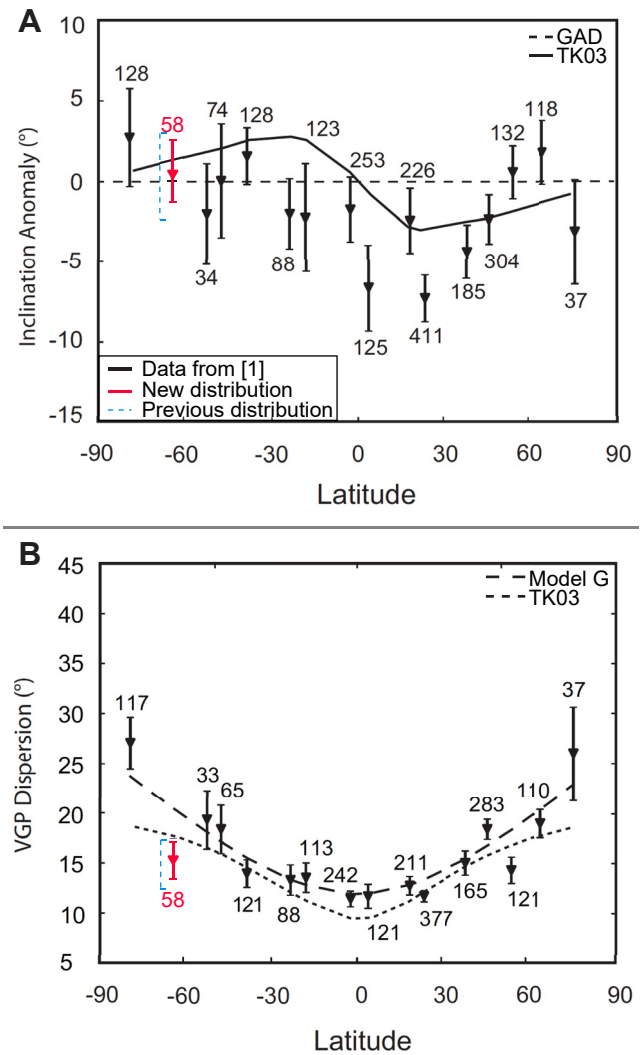

Figure 5. (a) Inclination anomaly and (b) VGP dispersion data from the PSV10 global data set, lightly modified from Cromwell et al. (2018). Data are organized into 10° latitude bins with average values shown with triangles and bootstrapped 95% confidence bounds shown with vertical bars. Red symbols show the new inclination anomaly and VGP dispersion estimates after incorporating data from this study and Kristjánsson et al. (2005). The original range of estimates by Cromwell et al. (2018) is shown in blue.

or younger, and most may be younger than ~15 ka (Baraldo et al., 2003; Oliva-Urcia et al., 2016; Smellie, 2021b). Based on their VGPs, the geomagnetic pole was over East Antarctica for much of this time.

After calculating paleomagnetic poles, we can also calculate the associated inclination anomaly (ΔI) and VGP dispersal (S_F). The expected ΔI and S_F will differ depending on which field model is used. Figure 5 shows our data (incorporated into the PSV10 global data set) and new values for ΔI and S_F in the 60°–70°S latitude bin. Overall, the new data are consistent with the TK03 field model, though the GAD model is not ruled out entirely. Notably, this latitude bin has very low VGP dispersion, but the reasons for this are not clear. After combining data from this study and previous studies, the AP data provide a long-term average of the geomagnetic field in this area, so insufficient time for VGP dispersal is not to blame. The S_F from only the JRI studies (Table S2 in Supporting Information S2) is not much higher than the S_F when including the Deception Island studies. The equivalent latitude bin in the northern hemisphere has a similar S_F of ~14° (Cromwell et al., 2018) compared to an S_F of 15.4° for the southern hemisphere (Table S2 in Supporting Information S2). This suggests that the convective regime of the core (probably related to the tangent cylinder; Christensen and Wicht, 2015) is the most likely explanation at this time.

5.3. JRIVG Stratigraphy

The basic volcanostratigraphy of the JRIVG has been established via previous volcanological and geochronological studies (see reviews by Haase & Beier, 2021; Smellie, 2021b). However, our data set allows for refinements and additions to that stratigraphy. The two uppermost igneous units at Taylor Bluff are the Forster Cliffs formation (2.5 Ma) and a tuff cone (~2 Ma; Figure S2a in Supporting Information S1, Table S1 in Supporting Information S2). However, the paleomagnetic directions from these units (Figure 3j) are unusual in similar ways (north-northwest declination, shallow inclination). We suggest that both units were erupted at ~2 Ma at this locality, which may require the creation of a new stratigraphic unit or incorporation of the columnar body that we sampled into the tuff cone unit. The 2.5 Ma age for the Forster Cliffs formation is from a different exposure to the east of Taylor Bluff (Smellie et al., 2013).

Two sites on Stickle Ridge were sampled by Kristjánsson et al. (2005) who found a reversed polarity and an age of 6.16 ± 0.08 Ma (assigned to the Lookalike Peaks formation). While this polarity and age are consistent with the geomagnetic timescale of Cande and Kent (1995), it is not consistent with the more-recent GTS 2020 timescale (Ogg, 2020) (Figure 6). The GTS 2020 timescale incorporates more recent data from more sources (including Cande and Kent (1995)), and therefore will be used here (Ogg, 2020). Regarding the Kristjánsson data from this period, a geomagnetic excursion may have been captured. The age determination is most likely accurate, because the paleomagnetic sites and the geochronology sampling site are at the same location.

In addition, all of the sites from Davies Dome yielded normal polarities in this study (Table 1). This conflicts with the determined age of the Kipling Mesa formation (5.36 ± 0.05 Ma), which is within the C3r chron, and not within error of a normal polarity period (Figure 6, Ogg, 2020). In this case, the disparity may be due to an incorrect age for the Kipling Mesa formation at this location. The 5.36 Ma age for this formation was determined at a different mesa to the southwest (Smellie et al., 2013), so it is possible that the flows here predate the assigned age for this unit.

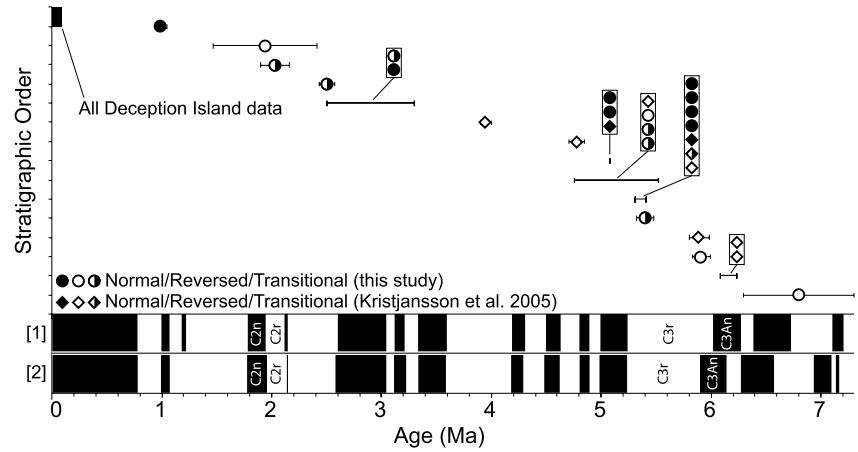

Figure 6. Compilation of polarity data from our sites and those of Kristjansson et al. (2005). (a) Geomagnetic polarity timescale of Ogg (2020). (b) Geomagnetic polarity timescale of Cande and Kent (1995). Stratigraphic order based on Smellie et al. (2013).

5.3.1. C2r/C2n Transition

Our paleomagnetic directional results most likely captured a geomagnetic reversal or excursion in this study, allowing for an accurate age determination of this event. Samples from the Taylor Bluff columnar body and tuff cone have transitional directions (Figure 3j), and their determined age (2.03 ± 0.13 Ma) overlaps with the C2r/C2n transition period (Figure 6). In addition, the measured paleointensities are among the lowest in the JRIVG (Table 2). As discussed earlier, the paleointensities should be interpreted with caution, but they are consistently low (Tables S9 and S10 in Supporting Information S2) and therefore support a transitional field in this case. Additional geochronological and paleomagnetic study of these units may help to place better temporal constraints on the C2r/C2n transition.

5.4. Paleointensity Determinations

Given the low success rates and non-ideal nature of our samples, we need to determine how many of our samples are accurate recorders of paleointensity. Sources of error in paleointensity experiments are numerous, often difficult to constrain, and vary depending on the technique that is used. We employed two methods that use heating steps (Thellier-Thellier and Tsunakawa-Shaw), and one method that involves no heating (pseudo-Thellier). Therefore, if similar paleointensities are determined between TT and PTT, or TS and PTT, then we can reasonably conclude that most of the error in the paleointensity determination is due to the sample itself and not due to the method that is employed. This in turn would increase our confidence in the measured paleointensities.

Figure 7a shows the measured paleointensities for samples that passed selection criteria from the PTT method and at least one other technique. Several samples from Keltie Head and Lachman Mesa show good agreement between the PTT and TS methods, suggesting that these results are the most reliable in our study. The Lachman Mesa flow 1 sites yields an average intensity of ~38 μT, which is expected under the long-term field model of Juarez et al. (1998) and Tauxe et al. (2013). The Keltie Head flow 1 site yields an average intensity of ~67 μT, which is more typical of the modern field. Four other sites (Davies Dome Flow 4, Lachman Mesa Flow 2, Smellie Peak Pillows, Smellie Peak Lapilli) have at least one sample that passed selection criteria from multiple methods (Figure 7a).

Results from different methods can also be compared at the site level, using averaged paleointensity values from multiple samples (Figure 7b). In general, results from TT experiments are systematically lower than results from PTT experiments at a given site. However, good agreement is found between TS and PTT experiments, as they fall near the 1:1 line in Figure 7b. Since the PTT method does not have heating steps, this suggests that the two heating steps in the TS method did not significantly alter the samples, as this would most likely cause some disagreement between the PTT and TS results. As stated earlier, some systemic errors are inherent to the samples themselves, and do not depend on the technique involved (e.g., Fe/Ti ratios), but this is largely beyond our control.

Table 2
Summary of Successful Paleointensity Results

Location	Site	Age[a]	*n*	Method	Intensity (μT)	St. Dev.
Davies Dome	Flow 1	5.36 ± 0.05	2	TT	25.0	6.1
	Flow 2	5.36 ± 0.05	3	TT, Shaw	42.5	6.0
	Flow 3	5.36 ± 0.05	3	Shaw	67.5	15.4
	Flow 4	5.36 ± 0.05	5	Shaw, PST	85.2	12.6
Humps Island	Neck	–	4	PST	10.4	18.5
Keltie Head	Flow 1	0.99 ± 0.05	11	TT, Shaw, PST	66.7[b]	3.4
	Flow 2	0.99 ± 0.05	4	Shaw	76.8	7.7
Lachman Mesa	Flow 1	5.04 ± 0.04	23	TT, Shaw, PST	38.1[b]	8.8
	Flow 2	5.04 ± 0.04	12	TT, Shaw, PST	44.2[b]	12.9
The Naze	Flow 2	–	2	TT	19.4	4.4
	Flow 3	–	1	PST	12.4	–
Seymour Island	Dike	6.8 ± 0.5	3	PST	7.9	1.6
Smellie Peak	Landslide Block	5.89 ± 0.09	1	PST	41.6	–
	Flow 1	5.14 ± 0.38	1	PST	14.0	–
	Flow 2	5.14 ± 0.38	1	PST	10.6	–
	Pillows	5.14 ± 0.38	11	Shaw, PST	7.9	5.4
	Scoria cone	5.91 ± 0.08	16	Shaw, PST	48.0	10.6
Taylor Bluff	Dike	1.94 ± 0.47	5	PST	60.8	7.6
	Columns	2.03 ± 0.13	10	Shaw, PST	5.3	2.6
	Tuff Cone	2.03 ± 0.13	17	PST	8.3	4.8

Note. St. Dev. = standard deviation; TT = Thellier-Thellier; Shaw = Tsunakawa-Shaw (LTD-DHT-Shaw); PST = pseudo-Thellier.

[a]See Table S1 in Supporting Information S1 for additional age information, see Smellie (2021b) for a compilation of ages from the JRIVG and associated references. [b]Does not include TT results.

However, given the level of agreement between these techniques, we conclude that their paleointensity results are generally reliable.

Finally, there are several sites that successfully passed the PTT *or* TS selection criteria, but not both. For example, samples from the tuff cone at Taylor Bluff yield an average paleointensity of ∼19 μT, but only pass the PTT selection criteria; we do not have any TS results from the same unit to compare them to. However, completely ignoring these results may amount to "throwing out" good data. As a compromise, we have plotted results from both methods in Figure 7c, highlighting which results are supported by multiple methods and which results are not. Sites with success in only one method should be interpreted with caution. Generally, there is a bimodal distribution of intensities, with most being >40 μT or <15 μT. This includes sites that are backed up by multiple methods. The reasons for this distribution are not entirely clear. It could be a product of the PTT and TS techniques themselves, or it could reflect an actual bimodal distribution of field strengths in the JRI area. Our results do not favor a continuation of modern field strength over the last 5 Ma, nor do they favor other models (Figure 7c; Juarez et al., 1998; Tauxe et al., 2013; Wang et al., 2015). Beyond this, more data is needed to make any definitive interpretations.

We recommend that future expeditions target the subaerial lava flows which are abundant in the JRIVG, but more difficult to access due to their exposures in steep cliff walls. The ideal paleointensity recorder, volcanic glass (Cromwell, Tauxe, Staudigel, & Ron, 2015), was not found in the places we were able to visit, and hence not sampled. Repeated glacial advances and retreats appear to have removed most flow tops where glass is normally located in subaerial flows. Despite these issues, it is entirely possible that future expeditions to the JRIVG will find volcanic glass, and better recovery of paleointensity data may result from such an expedition. Nevertheless, the rarity of any samples from the JRIVG and similar high-latitude locations motivates comparison to other

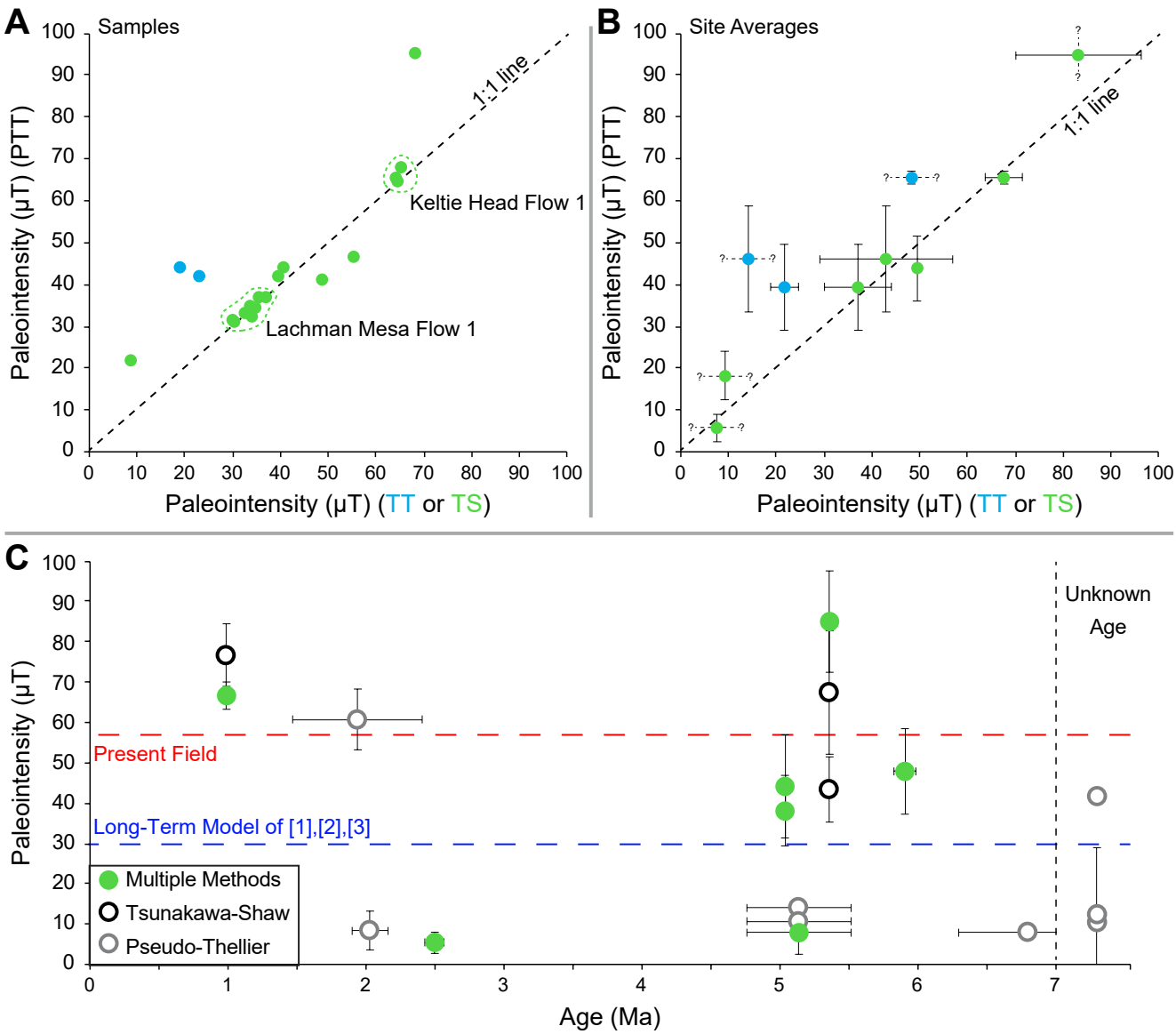

Figure 7. Comparison of paleointensity results from different techniques. (a) Results from different specimens of the same samples. Results from the pseudo-Thellier method (*y*-axis) and Tsunakawa-Shaw (green symbols, *x*-axis) or Thellier-Thellier method (blue symbols, *x*-axis) will ideally fall on the 1:1 line. (b) Average paleointensity results from different methods at the same sites. Symbols as in panel (a). (c) Average paleointensity results from each site. Symbols indicate if the site average includes results from multiple methods (filled symbols) or a single method (hollow symbols). [1] (Juarez et al., 1998); [2] (Tauxe et al., 2013); [3] (Wang et al., 2015).

datasets and to geomagnetic field models. An abundance of devitrified, altered volcanic glass can be found in the hyaloclastite breccias. But the hyaloclastite breccias have a complex thermal history (see Section 4.3.2), so paleointensity data from them will be of uncertain reliability.

6. Conclusions

We presented new paleomagnetic and paleointensity data from 31 sites in the James Ross Island volcanic group. These data give a long-term average of the geomagnetic field direction over the AP, especially when combined with a previous study of the JRIVG. Incorporation into the PSV10 field model (Cromwell et al., 2018) shows that anomalously low VGP dispersion seems to be a robust result and not an effect of sampling bias. We conclude that the low dispersion is a non-GAD effect, probably related to the tangent cylinder. We also found that revisions to

the stratigraphy at Taylor Bluff are probably necessary, and there are disparities between the measured polarities and measured ages at two localities (Stickle Ridge and Davies Dome). This study most likely found the C2r/C2n transition at Taylor Bluff, and the age of these units (2.03 ± 0.13 Ma) could be refined with further sampling and geochronological analysis to produce a well-constrained age of this event. Finally, results from paleointensity analysis should be interpreted with caution, but generally show a bimodal distribution of high- and low-intensities in the JRI area that do not favor or refute any current model of the high-latitude field. Two sites—Keltie Head Flow 1 and Lachman Mesa Flow 1—produced reliable paleointensity estimates of 67 and 38 μT, respectively.

More data are still needed to understand high-latitude geomagnetic field. In the long-term, we are limited by the few volcanic centers at high latitudes. In the short-term, gathering of further data is only limited by logistical concerns. We likely sampled ~10% of the exposed units in the JRIVG. A future expedition, that specifically targets the JRIVG for paleomagnetic and paleointensity sampling, is warranted, but would require extensive helicopter support. Additional absolute paleointensity data is still needed for this area, and any future study should make this a high priority. Specifically targeting the subaerial lava flows for directional data and targeting volcanic glass for paleointensity information will be the most successful approach.

Data Availability Statement

Tables S1–S10 in Supporting Information S2, which contain sample metadata, pole summaries, least-squares fits, paleointensity selection criteria, paleointensity results, and VGPs from previous studies, are available with the online version of this manuscript. A supplementary file containing additional descriptions of field locations, field photos, rock magnetics figures, demagnetization plots, and paleointensity figures is also available online. All paleomagnetic data are available via the MagIC database at https://earthref.org/MagIC/19313.

Acknowledgments
The authors would like to thank their fellow team members: Jennifer Buz, David Flannery, Ross Mitchell, Joe O'Rourke, Steve Skinner, Sarah Slotznick, David Smith, Frank Sousa, and Tom Tobin for their patience and assistance with sample collection. The authors also thank the crew of the Nathaniel B. Palmer and Air Center Helicopters for their logistical support. This work was funded by NSF Polar Programs grant ANT-1341729 to J. L. Kirschvink and an NSF EAR Postdoctoral Fellowship grant (2052963) to J. Biasi. The authors are not aware of any conflicts of interest that would affect this manuscript.

References

Baraldo, A., Rapalini, A. E., Böhnel, H., & Mena, M. (2003). Paleomagnetic study of Deception Island, South Shetland Islands, Antarctica. *Geophysical Journal International*, *153*, 333–343. https://doi.org/10.1046/j.1365-246x.2003.01881.x

Blundell, D. (1962). *Palaeomagnetic investigations in the Falkland Island dependencies* (p. 24). British Antarctic Survey.

Bowles, J. A., Jackson, M. J., Berquó, T. S., Sølheid, P. A., & Gee, J. S. (2013). Inferred time-and temperature-dependent cation ordering in natural titanomagnetites. *Nature Communications*, *4*, 1–9. https://doi.org/10.1038/ncomms2938

Calabozo, F. M., Strelin, J. A., Orihashi, Y., Sumino, H., & Keller, R. A. (2015). Volcano–ice–sea interaction in the Cerro Santa Marta area, northwest James Ross Island, Antarctic Peninsula. *Journal of Volcanology and Geothermal Research*, *297*, 89–108. https://doi.org/10.1016/j.jvolgeores.2015.03.011

Cande, S. C., & Kent, D. V. (1995). Revised calibration of the geomagnetic polarity timescale for the Late Cretaceous and Cenozoic. *Journal of Geophysical Research*, *100*, 6093–6095. https://doi.org/10.1029/94jb03098

Carrivick, J. L., Davies, B. J., Glasser, N. F., Nývlt, D., & Hambrey, M. J. (2012). Late-Holocene changes in character and behaviour of land-terminating glaciers on James Ross Island, Antarctica. *Journal of Glaciology*, *58*, 1176–1190. https://doi.org/10.3189/2012JoG11J148

Christensen, U. R., & Wicht, J. (2015). 8.10—Numerical dynamo simulations. In Schubert, G. (Ed.), *Treatise on Geophysics* (2nd ed., pp. 245–277). Elsevier. https://doi.org/10.1016/B978-0-444-53802-4.00145-7

Cottrell, E. (2015). Global distribution of active volcanoes. In *Volcanic hazards, risks and disasters* (pp. 1–16). Elsevier. https://doi.org/10.1016/b978-0-12-396453-3.00001-0

Cromwell, G., Johnson, C., Tauxe, L., Constable, C., & Jarboe, N. (2018). PSV10: A global data set for 0–10 Ma time-averaged field and paleosecular variation studies. *Geochemistry, Geophysics, Geosystems*, *19*. https://doi.org/10.1002/2017gc007318

Cromwell, G., Tauxe, L., & Halldórsson, S. (2015). New paleointensity results from rapidly cooled Icelandic lavas: Implications for Arctic geomagnetic field strength. *Journal of Geophysical Research: Solid Earth*, *120*, 2913–2934. https://doi.org/10.1002/2014jb011828

Cromwell, G., Tauxe, L., Staudigel, H., & Ron, H. (2015). Paleointensity estimates from historic and modern Hawaiian lava flows using glassy basalt as a primary source material. *Physics of the Earth and Planetary Interiors*, *241*, 44–56. https://doi.org/10.1016/j.pepi.2014.12.007

Cych, B., Morzfeld, M., & Tauxe, L. (2021). Bias Corrected Estimation of Paleointensity (BiCEP): An improved methodology for obtaining paleointensity estimates. *Geochemistry, Geophysics, Geosystems*, *22*, e2021GC009755. https://doi.org/10.1029/2021GC009755

Dalziel, I. W., Lawver, L. A., Norton, I. O., & Gahagan, L. M. (2013). The Scotia Arc: Genesis, evolution, global significance. *Annual Review of Earth and Planetary Sciences*, *41*. https://doi.org/10.1146/annurev-earth-050212-124155

De Groot, L., Biggin, A., Dekkers, M., Langereis, C., & Herrero-Bervera, E. (2013). Rapid regional perturbations to the recent global geomagnetic decay revealed by a new Hawaiian record. *Nature Communications*, *4*, 1–7. https://doi.org/10.1038/ncomms3727

Doubleday, P., Leat, P., Alabaster, T., Nell, P., & Tranter, T. (1994). Allochthonous oceanic basalts within the Mesozoic accretionary complex of Alexander Island, Antarctica: Remnants of proto-Pacific oceanic crust. *Journal of the Geological Society*, *151*, 65–78. https://doi.org/10.1144/gsjgs.151.1.0065

Drief, A., & Schiffman, P. (2004). Very low-temperature alteration of sideromelane in hyaloclastites and hyalotuffs from Kilauea and Mauna Kea volcanoes: Implications for the mechanism of palagonite formation. *Clays and Clay Minerals*, *52*, 622–634. https://doi.org/10.1346/ccmn.2004.0520508

Eagles, G. (2004). Tectonic evolution of the Antarctic–Phoenix plate system since 15 Ma. *Earth and Planetary Science Letters*, *217*, 97–109. https://doi.org/10.1016/s0012-821x(03)00584-3

Engel, Z., Nývlt, D., & Láska, K. (2012). Ice thickness, areal and volumetric changes of Davies Dome and Whisky Glacier (James Ross Island, Antarctic Peninsula) in 1979–2006. *Journal of Glaciology*, *58*, 904–914. https://doi.org/10.3189/2012JoG11J156

Esser, R. P., Kyle, P. R., & McIntosh, W. C. (2004). 40 Ar/39 Ar dating of the eruptive history of Mount Erebus, Antarctica: Volcano evolution. *Bulletin of Volcanology*, *66*, 671–686. https://doi.org/10.1007/s00445-004-0354-x

Evans, D. A. D. (2006). Proterozoic low orbital obliquity and axial-dipolar geomagnetic field from evaporite palaeolatitudes. *Nature*, *444*, 51–55. https://doi.org/10.1038/nature05203

Fuller, M., Cisowski, S., Hart, M., Haston, R., Schmidtke, E., & Jarrard, R. (1988). NRM: IRM (s) demagnetization plots: An aid to the interpretation of natural remanent magnetization. *Geophysical Research Letters*, *15*, 518–521. https://doi.org/10.1029/gl015i005p00518

Fuller, M., Kidane, T., & Ali, J. (2002). AF demagnetization characteristics of NRM, compared with anhysteretic and saturation isothermal remanence: An aid in the interpretation of NRM. *Physics and Chemistry of the Earth*, *27*, 1169–1177. https://doi.org/10.1016/s1474-7065(02)00127-4

Gehring, A., & Hofmeister, A. (1994). The transformation of lepidocrocite during heating: A magnetic and spectroscopic study. *Clays and Clay Minerals*, *42*, 409–415. https://doi.org/10.1346/ccmn.1994.0420405

Glatzmaier, G. A., & Roberts, P. H. (1995). A three-dimensional convective dynamo solution with rotating and finitely conducting inner core and mantle. *Physics of the Earth and Planetary Interiors*, *91*, 63–75. https://doi.org/10.1016/0031-9201(95)03049-3

Graham, J. W. (1949). The stability and significance of magnetism in sedimentary rocks. *Journal of Geophysical Research*, *54*, 131–167. https://doi.org/10.1029/JZ054i002p00131

Guyodo, Y., Bonville, P., Till, J. L., Ona-Nguema, G., Lagroix, F., & Menguy, N. (2016). Constraining the origins of the magnetism of lepidocrocite (γ-FeOOH): A Mössbauer and magnetization study. *Frontiers in Earth Science*, *4*, 28. https://doi.org/10.3389/feart.2016.00028

Haase, K. M., & Beier, C. (2021). *Bransfield Strait and James Ross Island: Petrology* (Vol. 55, pp. 285–301). Geological Society. https://doi.org/10.1144/M55-2018-37

Hill, D. J., Haywood, A. M., Valdes, P. J., Francis, J. E., Lunt, D. J., Wade, B. S., & Bowman, V. C. (2013). Paleogeographic controls on the onset of the Antarctic circumpolar current. *Geophysical Research Letters*, *40*, 5199–5204. https://doi.org/10.1002/grl.50941

Hole, M. (1988). Post-subduction alkaline volcanism along the Antarctic Peninsula. *Journal of the Geological Society*, *145*, 985–998. https://doi.org/10.1144/gsjgs.145.6.0985

Hole, M., & Larter, R. D. (1993). Trench-proximal volcanism following ridge crest-trench collision along the Antarctic Peninsula. *Tectonics*, *12*, 897–910. https://doi.org/10.1029/93tc00669

Hole, M., Smellie, J. L., & Marriner, G. (1991). Geochemistry and tectonic setting of Cenozoic alkaline basalts from Alexander Island, Antarctic Peninsula. In *International Symposium on Antarctic Earth Sciences* (Vol. 5, pp. 521–526).

Johnson, C. L., & Constable, C. G. (1995). The time-averaged geomagnetic field as recorded by lava flows over the past 5 Myr. *Geophysical Journal International*, *122*, 489–519. https://doi.org/10.1111/j.1365-246X.1995.tb07010.x

Johnson, C. L., Constable, C. G., Tauxe, L., Barendregt, R., Brown, L. L., Coe, R. S., et al. (2008). Recent investigations of the 0–5 Ma geomagnetic field recorded by lava flows. *Geochemistry, Geophysics, Geosystems*, *9*. https://doi.org/10.1029/2007GC001696

Johnson, C. L., & McFadden, P. (2015). 5.11—The time-averaged field and paleosecular variation. In Schubert, G. (Ed.), *Treatise on Geophysics* (2nd ed, pp. 385–417). Elsevier. https://doi.org/10.1016/B978-0-444-53802-4.00105-6

Johnson, H., Lowrie, W., & Kent, D. (1975). Stability of ARM in fine and course grained magnetite and maghemite particles. *Geophysical Journal of the Royal Astronomical Society*, *41*, 1–10. https://doi.org/10.1111/j.1365-246x.1975.tb05480.x

Jokat, W., Boebel, T., König, M., & Meyer, U. (2003). Timing and geometry of early Gondwana breakup. *Journal of Geophysical Research*, *108*. https://doi.org/10.1029/2002jb001802

Juarez, M., Tauxe, L., Gee, J., & Pick, T. (1998). The intensity of the Earth's magnetic field over the past 160 million years. *Nature*, *394*, 878–881. https://doi.org/10.1038/29746

Kirschvink, J. (1980). The least-squares line and plane and the analysis of palaeomagnetic data. *Geophysical Journal International*, *62*, 699–718. https://doi.org/10.1111/j.1365-246X.1980.tb02601.x

Kirschvink, J. L., Kopp, R. E., Raub, T. D., Baumgartner, C. T., & Holt, J. W. (2008). Rapid, precise, and high-sensitivity acquisition of paleomagnetic and rock-magnetic data: Development of a low-noise automatic sample changing system for superconducting rock magnetometers. *Geochemistry, Geophysics, Geosystems*, *9*. https://doi.org/10.1029/2007GC001856

Košler, J., Magna, T., Mlčoch, B., Mixa, P., Nỳvlt, D., & Holub, F. (2009). Combined Sr, Nd, Pb and Li isotope geochemistry of alkaline lavas from northern James Ross Island (Antarctic Peninsula) and implications for back-arc magma formation. *Chemical Geology*, *258*, 207–218.

Kristjansson, L., Gudmundsson, M., Smellie, J. L., McIntosh, W. C., & Esser, R. (2005). Palaeomagnetic, 40Ar/39Ar, and stratigraphical correlation of Miocene-Pliocene basalts in the Brandy Bay area. *James Ross Island, Antarctica: Antarctic Science*, *17*, 409–417. https://doi.org/10.1017/s0954102005002853

Lawrence, K., Tauxe, L., Staudigel, H., Constable, C., Koppers, A., McIntosh, W., & Johnson, C. (2009). Paleomagnetic field properties at high southern latitude. *Geochemistry, Geophysics, Geosystems*, *10*. https://doi.org/10.1029/2008gc002072

Livermore, P. W., Finlay, C. C., & Bayliff, M. (2020). Recent north magnetic pole acceleration towards Siberia caused by flux lobe elongation. *Nature Geoscience*, *13*, 387–391. https://doi.org/10.1038/s41561-020-0570-9

Livermore, P. W., Hollerbach, R., & Finlay, C. C. (2017). An accelerating high-latitude jet in Earth's core. *Nature Geoscience*, *10*, 62–68. https://doi.org/10.1038/ngeo2859

Lowrie, W., & Fuller, M. (1971). On the alternating field demagnetization characteristics of multidomain thermoremanent magnetization in magnetite. *Journal of Geophysical Research*, *76*, 6339–6349. https://doi.org/10.1029/jb076i026p06339

Mankinen, E. A., & Cox, A. (1988). Paleomagnetic investigation of some volcanic rocks from the McMurdo volcanic province, Antarctica. *Journal of Geophysical Research*, *93*, 11599–11612. https://doi.org/10.1029/JB093iB10p11599

Marenssi, S. A., Casadío, S., & Santillana, S. N. (2010). Record of Late Miocene glacial deposits on Isla Marambio (Seymour Island). *Antarctic Peninsula: Antarctic Science*, *22*, 193–198. https://doi.org/10.1017/s0954102009990629

McElhinny, M. W., & McFadden, P. L. (1997). Palaeosecular variation over the past 5 Myr based on a new generalized database. *Geophysical Journal International*, *131*, 240–252. https://doi.org/10.1111/j.1365-246x.1997.tb01219.x

Merrill, R. T., & McFadden, P. L. (2003). The geomagnetic axial dipole field assumption. *Physics of the Earth and Planetary Interiors*, *139*, 171–185. https://doi.org/10.1016/j.pepi.2003.07.016

Milanese, F., Rapalini, A., Slotznick, S. P., Tobin, T. S., Kirschvink, J., & Olivero, E. (2019). Late Cretaceous paleogeography of the Antarctic Peninsula: New paleomagnetic pole from the James Ross Basin. *Journal of South American Earth Sciences*, *91*, 131–143. https://doi.org/10.1016/j.jsames.2019.01.012

Milanese, F. N., Olivero, E. B., Slotznick, S. P., Tobin, T. S., Raffi, M. E., Skinner, S. M., et al. (2020). Coniacian-Campanian magnetostratigraphy of the Marambio Group: The Santonian-Campanian boundary in the Antarctic Peninsula and the complete Upper Cretaceous–Lowermost Paleogene chronostratigraphical framework for the James. *Ross Basin: Palaeogeography, Palaeoclimatology, Palaeoecology*, *555*, 109871. https://doi.org/10.1016/j.palaeo.2020.109871

Minyuk, P., Subbotnikova, T., & Plyashkevich, A. (2011). Measurements of thermal magnetic susceptibility of hematite and goethite: Izvestiya. *Physics of the Solid Earth*, *47*, 762–774. https://doi.org/10.1134/s1069351311080052

Muxworthy, A., & McClelland, E. (2000). Review of the low-temperature magnetic properties of magnetite from a rock magnetic perspective. *Geophysical Journal International*, *140*, 101–114. https://doi.org/10.1046/j.1365-246x.2000.00999.x

Nayudu, Y. R. (1964). Palagonite tuffs (hyaloclastites) and the products of post-eruptive processes. *Bulletin Volcanologique*, *27*, 391–410. https://doi.org/10.1007/bf02597539

Ogg, J. G. (2020). Chapter 5: Geomagnetic polarity time scale. In Gradstein, F. M., Ogg, J. G., Schmitz, M. D., & Ogg, G. M. (Eds.), *Geologic time scale 2020* (pp. 159–192). Elsevier. https://doi.org/10.1016/B978-0-12-824360-2.00005-X

Oliva-Urcia, B., Gil-Peña, I., Maestro, A., López-Martínez, J., Galindo-Zaldívar, J., Soto, R., et al. (2016). Paleomagnetism from Deception Island (South Shetlands archipelago, Antarctica), new insights into the interpretation of the volcanic evolution using a geomagnetic model. *International Journal of Earth Sciences*, *105*, 1353–1370. https://doi.org/10.1007/s00531-015-1254-3

Olivero, E. B. (2012). Sedimentary cycles, ammonite diversity and palaeoenvironmental changes in the Upper Cretaceous Marambio Group, Antarctica. *Cretaceous Research*, *34*, 348–366. https://doi.org/10.1016/j.cretres.2011.11.015

Özdemir, Ö., & Dunlop, D. J. (1996). Thermoremanence and Néel temperature of goethite. *Geophysical Research Letters*, *23*, 921–924. https://doi.org/10.1029/96GL00904

Pankhurst, R. (1982). Rb-Sr geochronology of Graham Land, Antarctica. *Journal of the Geological Society*, *139*, 701–711. https://doi.org/10.1144/gsjgs.139.6.0701

Paterson, G. A., Heslop, D., & Pan, Y. (2016). The pseudo-Thellier palaeointensity method: New calibration and uncertainty estimates. *Geophysical Journal International*, *207*, 1596–1608. https://doi.org/10.1093/gji/ggw349

Porreca, M., Cifelli, F., Soriano, C., Giordano, G., Romano, C., Conticelli, S., & Mattei, M. (2014). Hyaloclastite fragmentation below the glass transition: An example from El Barronal submarine volcanic complex (Spain). *Geology*, *42*, 87–90. https://doi.org/10.1130/g34744.1

Riley, T. R., & Leat, P. T. (2021). *Palmer Land and Graham Land Volcanic Groups (Antarctic Peninsula): Volcanology* (Vol. 55). Geological Society. https://doi.org/10.1144/m55-2018-36

Roberts, E. M., Lamanna, M. C., Clarke, J. A., Meng, J., Gorscak, E., Sertich, J. J., et al. (2014). Stratigraphy and vertebrate paleoecology of Upper Cretaceous–lowest Paleogene strata on Vega Island, Antarctica. *Palaeogeography, Palaeoclimatology, Palaeoecology*, *402*, 55–72. https://doi.org/10.1016/j.palaeo.2014.03.005

Scharnberger, C., Scharon, L., & Craddock, C. (1982). In Craddock, C. (Ed.), *Paleomagnetism of rocks from Graham Land and western Ellsworth Land, Antarctica: Antarctic Geoscience* (pp. 371–375).

Scher, H. D., Whittaker, J. M., Williams, S. E., Latimer, J. C., Kordesch, W. E., & Delaney, M. L. (2015). Onset of Antarctic Circumpolar Current 30 million years ago as Tasmanian Gateway aligned with westerlies. *Nature*, *523*, 580–583. https://doi.org/10.1038/nature14598

Smellie, J., Johnson, J., & Nelson, A. (2013). *Geological Map of James Ross Island. 1. James Ross Island Volcanic group: BAS GEOMAP 2 Series Sheet 5*. Cambridge, UK: British Antarctic Survey. Retrieved from http://nora.nerc.ac.uk/506743/1/BAS%20GEOMAP%202%2C%20sheet%205%20-%20Geological%20map%20of%20James%20Ross%20Island%20-%20I%20-%20James%20Ross%20Island%20volcanic%20group.pdf

Smellie, J. L. (1987). Geochemistry and tectonic setting of alkaline volcanic rocks in the Antarctic Peninsula: A review. *Journal of Volcanology and Geothermal Research*, *32*, 269–285. https://doi.org/10.1016/0377-0273(87)90048-5

Smellie, J. L. (2021a). *Antarctic Volcanism: Volcanology and Palaeoenvironmental Overview*. Geological Society. https://doi.org/10.1144/m55-2020-1

Smellie, J. L. (2021b). *Bransfield Strait and James Ross Island: Volcanology* (pp. 227–284). Geological Society. https://doi.org/10.1144/M55-2018-58

Smellie, J. L., & Hole, M. J. (2021). *1a Antarctic Peninsula: Volcanology* (pp. 305–325). Geological Society. https://doi.org/10.1144/M55-2018-59

Smellie, J. L., Johnson, J. S., McIntosh, W., Esser, R., Gudmundsson, M., Hambrey, M. J., & De Vries, B. (2008). Six million years of glacial history recorded in volcanic lithofacies of the James Ross Island Volcanic Group. *Antarctic Peninsula: Palaeogeography, Palaeoclimatology, Palaeoecology*, *260*, 122–148. https://doi.org/10.1016/j.palaeo.2007.08.011

Smellie, J. L., & Martin, A. P. (2021). *Erebus Volcanic Province: Volcanology* (pp. 415–446). Geological Society. https://doi.org/10.1144/M55-2018-62

Sykes, M. A. (1988). *The petrology and tectonic significance of the James Ross Island volcanic group, Antarctica*. University of Nottingham.

Tauxe, L., Gans, P., & Mankinen, E. A. (2004). Paleomagnetism and 40Ar/39Ar ages from volcanics extruded during the Matuyama and Brunhes Chrons near McMurdo Sound, Antarctica. *Geochemistry, Geophysics, Geosystems*, *5*. https://doi.org/10.1029/2003GC000656

Tauxe, L., Gee, J., Steiner, M., & Staudigel, H. (2013). Paleointensity results from the Jurassic: New constraints from submarine basaltic glasses of ODP Site 801C. *Geochemistry, Geophysics, Geosystems*, *14*, 4718–4733. https://doi.org/10.1002/ggge.20282

Tauxe, L., & Kent, D. V. (2004). A simplified statistical model for the geomagnetic field and the detection of shallow bias in paleomagnetic inclinations: Was the ancient magnetic field dipolar? *Timescales of the Paleomagnetic Field, Geophysical Monograph Series*, *145*, 101–115.

Tauxe, L., Mullender, T., & Pick, T. (1996). Potbellies, wasp-waists, and superparamagnetism in magnetic hysteresis. *Journal of Geophysical Research*, *101*, 571–583. https://doi.org/10.1029/95jb03041

Tauxe, L., Pick, T., & Kok, Y. (1995). Relative paleointensity in sediments: A pseudo-Thellier approach. *Geophysical Research Letters*, *22*, 2885–2888. https://doi.org/10.1029/95gl03166

Tauxe, L., Shaar, R., Jonestrask, L., Swanson-Hysell, N., Minnett, R., Koppers, A., et al. (2016). PmagPy: Software package for paleomagnetic data analysis and a bridge to the Magnetics Information Consortium (MagIC) database. *Geochemistry, Geophysics, Geosystems*, *17*, 2450–2463. https://doi.org/10.1002/2016GC006307

Thellier, E., & Thellier, O. (1959). Sur l'intensité du champ magnétique terrestre dans le passé historique et géologique. *Annales Geophysicae*, *15*, 285–376.

Tobin, T. S., Roberts, E. M., Slotznick, S. P., Biasi, J. A., Clarke, J. A., O'Connor, P. M., et al. (2020). New evidence of a Campanian age for the Cretaceous fossil-bearing strata of Cape Marsh, Robertson Island, Antarctica. *Cretaceous Research*, *108*, 104313. https://doi.org/10.1016/j.cretres.2019.104313

Tobin, T. S., Ward, P. D., Steig, E. J., Olivero, E. B., Hilburn, I. A., Mitchell, R. N., et al. (2012). Extinction patterns, δ18O trends, and magnetostratigraphy from a southern high-latitude Cretaceous–Paleogene section: Links with Deccan volcanism. *Palaeogeography, Palaeoclimatology, Palaeoecology*, *350–352*, 180–188. https://doi.org/10.1016/j.palaeo.2012.06.029

Torsvik, T. H., Gaina, C., & Redfield, T. F. (2007). *Antarctica and global paleogeography: From Rodinia, rhrough Gondwanaland and Pangea, to the birth of the Southern Ocean and the opening of gateways: Open-File Report Report 2007-1047-KP-11* (pp. 125–140). https://doi.org/10.3133/ofr20071047KP11

Turnbull, G. (1959). Some palaeomagnetic measurements in Antarctica. *Arctic*, *12*, 151–157. https://doi.org/10.14430/arctic3722

Valencio, D., & Fourcade, N. H. (1969). Estudio paleomagnetico y petrografico de algunas formaciones cenozoicas de las islas shetland de sur. *Antártico Argentino*, *125*, 25.

Vandamme, D. (1994). A new method to determine paleosecular variation. *Physics of the Earth and Planetary Interiors*, *85*, 131–142. https://doi.org/10.1016/0031-9201(94)90012-4

Veikkolainen, T., Pesonen, L., & Korhonen, K. (2014). An analysis of geomagnetic field reversals supports the validity of the Geocentric Axial Dipole (GAD) hypothesis in the Precambrian. *Precambrian Supercontinents*, *244*, 33–41. https://doi.org/10.1016/j.precamres.2013.10.009

Wang, H., Kent, D. V., & Rochette, P. (2015). Weaker axially dipolar time-averaged paleomagnetic field based on multidomain-corrected paleointensities from Galapagos lavas. *Proceedings of the National Academy of Sciences*, *112*, 15036–15041. https://doi.org/10.1073/pnas.1505450112

Watson, G. S. (1956). A test for randomness of directions. *Geophysical Supplements to the Monthly Notices of the Royal Astronomical Society*, *7*, 160–161. https://doi.org/10.1111/j.1365-246X.1956.tb05561.x

Xu, S., & Dunlop, D. J. (1995). Toward a better understanding of the Lowrie-Fuller test. *Journal of Geophysical Research*, *100*, 22533–22542. https://doi.org/10.1029/95jb02154

Yamagishi, H., & Dimroth, E. (1985). A comparison of Miocene and Archean rhyolite hyaloclastites: Evidence for a hot and fluid rhyolite lava. *Journal of Volcanology and Geothermal Research*, *23*, 337–355. https://doi.org/10.1016/0377-0273(85)90040-x

Yamamoto, Y., & Yamaoka, R. (2018). Paleointensity study on the Holocene surface lavas on the island of Hawaii using the Tsunakawa–Shaw method. *Frontiers in Earth Science*, *6*, 48. https://doi.org/10.3389/feart.2018.00048

Yu, Y., Tauxe, L., & Genevey, A. (2004). Toward an optimal geomagnetic field intensity determination technique. *Geochemistry, Geophysics, Geosystems*, *5*. https://doi.org/10.1029/2003gc000630